Published in final edited form as:
Nature. 2017 October 26; 550(7677): 539–542. doi:10.1038/nature24046.

Nucleosome-Chd1 structure and implications for chromatin remodelling

Lucas Farnung[1], **Seychelle M. Vos**[1], **Christoph Wigge**[1], and **Patrick Cramer**[1]
[1]Max Planck Institute for Biophysical Chemistry, Department of Molecular Biology, Am Fassberg 11, 37077 Göttingen, Germany

Abstract

Chromatin remodelling factors change nucleosome positioning and facilitate DNA transcription, replication, and repair1. The conserved remodelling factor Chd12 can shift nucleosomes and induce a regular nucleosome spacing3–5. Chd1 is required for RNA polymerase II passage through nucleosomes6 and for cellular pluripotency7. Chd1 contains the DNA-binding domains SANT and SLIDE, a bilobal motor domain that hydrolyses adenosine triphosphate (ATP), and a regulatory double chromodomain. Here we report the cryo-electron microscopy (cryo-EM) structure of Chd1 from the yeast *S. cerevisiae* bound to a nucleosome at a resolution of 4.8 Å. Chd1 detaches two turns of DNA from the histone octamer and binds between the two DNA gyres in a state poised for catalysis. The SANT and SLIDE domains contact detached DNA around superhelical location (SHL) -7 of the first DNA gyre. The ATPase motor binds the second DNA gyre at SHL +2 and is anchored to the N-terminal tail of histone H4 as in a recent nucleosome-Snf2 ATPase structure8. Comparison with published results9 reveals that the double chromodomain swings towards nucleosomal DNA at SHL +1, resulting in ATPase closure. The ATPase can then promote translocation of DNA towards the nucleosome dyad, thereby loosening the first DNA gyre and remodelling the nucleosome. Translocation may involve ratcheting of the two lobes of the ATPase, which is trapped in a pre- or post-translocated state in the absence8 or presence, respectively, of transition state-mimicking compounds.

To investigate how RNA polymerase II transcribes through chromatin, we prepared factors that facilitate chromatin transcription in the yeast *S. cerevisiae* (Methods). These included the chromatin-remodelling enzyme Chd1 (chromodomain-helicase-DNA binding protein 1), the histone chaperone FACT (facilitates chromatin transcription) and the transcription elongation factor Paf1C (polymerase-associated factor 1 complex). We formed a complex of these factors in the presence of the transition state-mimicking adduct ADP·BeF_3 and a

Correspondence and requests for materials should be addressed to PC (pcramer@mpibpc.mpg.de).

Author contributions LF designed and carried out experiments and performed cryo-EM data acquisition and analysis. SMV developed the protein expression strategy, performed baculovirus production, and insect cell expression. CW assisted with cryo-EM grid preparation and data collection. PC designed and supervised research. LF and PC interpreted the data and wrote the manuscript, with input from all authors.

Author information The electron density reconstruction and final model were deposited with the EM Data Base (accession code EMDB-3765) and with the Protein Data Bank (accession code 5O9G).

The authors declare no competing financial interest.

Europe PMC Funders Author Manuscripts

nucleosome with DNA comprising the Widom 601 sequence10 and 63 base pairs (bp) of extranucleosomal DNA (Methods, Extended Data Fig. 1a).

Cryo-EM analysis revealed nucleosome-Chd1 particles that had lost FACT and Paf1C (Methods, Extended Data Fig. 1b-d). The resulting reconstruction of the nucleosome-Chd1 complex at an overall resolution of 4.8 Å revealed protein secondary structure (Extended Data Fig. 2, Supplemental Video 1). Crystal structures of the nucleosome10,11 and Chd1 domains12,13 were unambiguously placed into the density. Only a minor, unassigned density remained that was located near histones H3 (residues 46-56) and H2A (residues 56-71) and may arise from a C-terminal domain14 in Chd1. A detailed structure was obtained after flexible fitting and real-space refinement.

The structure reveals an altered nucleosome with one engaged Chd1 molecule (Fig. 1). Two turns of nucleosomal DNA at SHL -5 to -7 are detached from the histone octamer. This alters the trajectory of extranucleosomal DNA by ~60° and breaks DNA interactions with histones H2A, H2B, and H3 (Fig. 2a). The ability of Chd1 to detach DNA depends on the presence of an ATP analogue or ADP·$BeF_3$15, indicating that our structure trapped Chd1 in a state poised for activity. The histone octamer is unaltered compared to the free nucleosome, whereas it adopts an altered conformation in a nucleosome-ACF remodelling complex with ADP·$BeF_3$16 (Extended Data Fig. 2g).

Chd1 binds between extranucleosomal DNA and the second DNA gyre at SHL +2 (Fig. 2, Extended Data Fig. 3), consistent with lower-resolution information15. Chd1 domains assemble between the two DNA gyres and form multiple DNA interactions. The SANT and SLIDE domains contribute to Chd1 affinity for the nucleosome17 and contact the first turn of extranucleosomal DNA in a way that was observed for free DNA13. The ATPase engages with DNA at SHL +2, consistent with the structure of the related Snf2 ATPase bound to the nucleosome8 and with biochemical data9,17. The double chromodomain contacts DNA at SHL +1 (Extended Data Fig. 3b) and binds between the SANT domain and ATPase lobe 1. The structure is incompatible with binding of linker histone H118, explaining why H1 can repress Chd1-dependent remodelling5.

The ATPase motor adopts a closed conformation with the ADP·BeF_3 adduct bound between lobes 1 and 2 (Fig. 3b). Compared to the free Chd1 structure12, lobe 2 rotates by ~40° towards lobe 1. This rotation closes the active site and positions the catalytic19,20 arginine ‘fingers’ in lobe 2 (R804 and R807) close to the ATP-binding site (Extended Data Fig. 3e). One of these arginine fingers is mutated in human CHD1 in prostate cancers21. These observations indicate that the structure trapped Chd1 in a functional state poised for catalysis.

The ATPase motor interacts extensively with DNA (Fig. 2b, Extended Data Fig. 3a-c). Based on biochemical and structural observations9,22, we define the ‘tracking strand’ as the DNA strand running in the 5’ to 3’ direction from SHL +2 towards the histone octamer dyad. Lobe 1 contacts the tracking strand backbone with three protein regions containing ATPase motifs Ia and Ic, and with a loop (residues 457-461) located between motifs Ia and Ib. The lobe 1 regions formed by motifs IIa and III contact the complementary ‘guide’ DNA strand. Lobe 2

interacts with the tracking strand via loops formed by motifs IV, IVa, and V. Residue Trp793 in motif Va inserts into the minor groove and contacts the guide strand backbone (Extended Data Fig. 3f). These ATPase-DNA interactions resemble the 'primary' interactions in a nucleosome-Snf2 complex8 and interactions observed in a distantly related ATPase-DNA complex23. The interactions support the model that Chd1 translocates along the DNA minor groove from SHL +2 away from the octamer dyad, thereby moving DNA towards the dyad1,9,24.

Comparison of our structure with the nucleosome-Snf2 complex8 suggests a model for how ATP binding and hydrolysis result in DNA translocation (Supplemental Video 3). In the absence of ATP8, the ATPase is partially closed, whereas in the presence of ADP·BeF_3 it is entirely closed (Extended Data Fig. 3e). Superposition of lobe 1 in these two structures results in different positions of lobe 2, which are offset along DNA by approximately one base pair in the direction of translocation (Fig. 2b). Provided that ATPases move in steps of one base pair22,25,26, these observations suggest that the conformational 'ratcheting' between the ATPase lobes underlies DNA translocation27.

According to this translocation model, the ATPase first binds DNA in a partially closed conformation (pre-translocation state). ATP binding then leads to complete closure of the ATPase and lobe 2 movement, which triggers DNA translocation by one base pair (post-translocation state). ATP hydrolysis then dissociates ADP and resets the ATPase to the pre-translocated state at the new DNA position. We speculate that directional translocation within this enzymatic cycle results from non-equivalent lobe 2 movements during translocation and ATPase resetting.

The structure also reveals the basis for ATPase activation by nucleosome binding (Fig. 3a). In the absence of the nucleosome, ATPase lobe 2 is sequestered in an open conformation by the 'chromo-wedge', an acidic region in the double chromodomain12. In the presence of the nucleosome, the double chromodomain swings by 15° and binds nucleosomal DNA9. The chromo-wedge contacts the DNA backbone at SHL +1 (Extended Data Fig. 3b) using a region that contains cancer mutations in the human homologue CHD428. Thus, binding of Chd1 to nucleosomal DNA induces swinging of the double chromodomain that releases lobe 2 and allows for ATPase closure and activation (Supplemental Video 2). Chd1 recognizes bent nucleosomal DNA because free DNA only weakly activates the ATPase12, and straight B-DNA would clash with the double chromodomain (Extended Data Fig. 3d).

Interactions of the double chromodomain with other Chd1 domains may compensate for the loss of histone-DNA contacts upon detaching nucleosomal DNA. The double chromodomain binds the SLIDE domain as predicted9 (Extended Data Fig. 3g). It also binds and buttresses lobe 1, which not only contacts SHL +2 but also detached DNA around SHL -6 on the second DNA gyre (Extended Data Fig. 3c). In particular, motif Ib and residue 506 (between motifs Ic and II) bind the DNA backbone. These additional contacts between the ATPase and the second DNA gyre resemble the 'secondary' contacts in the nucleosome-Snf2 complex8.

Our structure also reveals Chd1 interactions with histones. ATPase lobe 2 contacts highly conserved residues in helix α1 of histone H3. Lobe 2 also uses an acidic pocket to bind to

the basic N-terminal tail of histone H4 (Extended Data Fig. 4a). This predicts that H4 acetylation or methylation at residues K16 and K20, respectively, alter Chd1 binding. A similar lobe 2-H4 tail interaction is observed in the nucleosome-Snf2 complex8, and the H4-binding pocket is conserved in ISWI29, suggesting that H4 tail binding is a general feature of remodelling enzymes.

Our structural observations and published biochemical data9,15,17,24,30 converge on a model for nucleosome remodelling by Chd1 (Extended Data Fig. 4b). Chd1 positions its ATPase motor at SHL +2 and uses a ratcheting cycle to move on the tracking strand in the 3'-5' direction away from the octamer dyad. As Chd1 holds onto histones, this results in DNA translocation towards the octamer dyad. Progression of the ATPase by one nucleotide per catalytic event22,25,26 leads to a helical rotation of DNA. This may generate a short DNA region that is slightly peeled away from the octamer surface. Propagation of this dissociated region would reposition the octamer, consistent with proposed models1,31.

This model for nucleosome remodelling, however, does not explain how Chd1 centers nucleosomes on a DNA fragment and how it induces a regular nucleosome spacing. One possibility9 is that two Chd1 molecules act from opposite sides of the nucleosome to center it by shifting it away from both DNA ends. Alternatively, a single Chd1 molecule may center the nucleosome if the ATPase motor17 could swing between two positions on the nucleosome. It is also possible that instead or in addition the DNA-binding region can be repositioned as observed for SNF2h32.

In conclusion, our structure of the nucleosome-Chd1 complex provides a framework for understanding nucleosome remodelling and its coupling to other nuclear events. The conservation of Chd1 domains across species and homologues indicates that our results are relevant for understanding all proteins of the CHD family. The high conservation of the ATPase motor (Extended Data Fig. 4c) further suggests that our results can inform mechanistic analysis of other chromatin-remodelling factors, including those of the ISWI family33, which resemble Chd1 in domain architecture.

Methods

Cloning and protein expression

A vector encoding full-length *S. cerevisiae* Chd1 was obtained through the MRC PPU Reagents and Services facility (MRC PPU, College of Life Sciences, University of Dundee, Scotland). The vector was used as a PCR template for cloning Chd1 into a modified pFastBac vector via ligation independent cloning (LIC) [a gift of Scott Gradia, UC Berkeley, vector 438-C (Addgene: 55220)]. The construct contains an N-terminal 6x His tag followed by a maltose binding protein (MBP) tag and a tobacco etch virus protease cleavage site. gBlocks encoding *Trichoplusia ni* codon-optimized Spt16 and Pob3 were designed using Integrated DNA Technologies (IDT) Codon Optimization Tool and synthesized by IDT. Two gBlocks encoding the N- and C-terminal part of Spt16 were cloned into vector 438-C using CPEC. Paf1C constructs have been previously described 35. The gBlock encoding Pob3 was cloned into vector 438-A (Addgene: 55218) using LIC. Combination of Spt16 and Pob3 on a single vector was achieved by using successive rounds of LIC. Each subunit is preceded by a

PolH promoter and followed by a SV40 termination site. Spt16 has an N-terminal 6x His tag, followed by a maltose binding protein (MBP) tag, and a tobacco etch virus protease cleavage site.

Purified plasmids (500 ng) were electroporated into DH10EMBacY (Geneva Biotech, Geneva, Switzerland) cells to generate bacmids containing full-length Chd1 or FACT constructs. Bacmids were prepared from positive clones using blue/white selection and isopropanol precipitation. V0, and V1 virus productions were performed as described34. 600 mL of Hi5 cells grown in ESF-921 media (Expression Systems, Davis, CA, United States) were infected with 300 μL of V1 virus for protein expression. The cells were grown for 48-72 hrs at 27 °C. Cells were harvested by centrifugation (238 xg, 4°C, 30 min) and resuspended in lysis buffer (300 mM NaCl, 20 mM Na•HEPES pH 7.4, 10% glycerol (v/v), 1 mM DTT, 30 mM imidazole pH 8.0, 0.284 μg/ml leupeptin, 1.37 μg/ml pepstatin A, 0.17 mg/ml PMSF, 0.33 mg/ml benzamidine). The cell resuspension was snap frozen and stored at -80 °C.

Protein purification

Protein purifications were performed at 4 °C. Frozen cell pellets were thawed and lysed by sonication. Lysates were cleared by centrifugation (18,000 xg, 4 °C, 30 min) and ultracentrifugation (235,000 xg, 4°C, 60 min). The supernatant containing Chd1 was filtered using 0.8 μm syringe filters (Millipore) and applied onto a GE HisTrap HP 5 mL (GE Healthcare, Little Chalfont, United Kingdom), pre-equilibrated in lysis buffer. After sample application, the column was washed with 10 CV lysis buffer, 5 CV high salt buffer (1 M NaCl, 20 mM Na•HEPES pH 7.4, 10% glycerol (v/v), 1 mM DTT, 30 mM imidazole pH 8.0, 0.284 μg/ml leupeptin, 1.37 μg/ml pepstatin A, 0.17 mg/ml PMSF, 0.33 mg/ml benzamidine), and 5 CV lysis buffer. The protein was eluted with a gradient of 0-100% elution buffer (300 mM NaCl, 20 mM Na•HEPES pH 7.4, 10% glycerol (v/v), 1 mM DTT, 500 mM imidazole pH 8.0, 0.284 μg/ml leupeptin, 1.37 μg/ml pepstatin A, 0.17 mg/ml PMSF, 0.33 mg/ml benzamidine). Peak fractions were pooled and dialyzed for 16 hours against 600 mL dialysis buffer (300 mM NaCl, 20 mM Na•HEPES pH 7.4, 10% glycerol (v/v), 1 mM DTT, 30 mM imidazole) in the presence of 2 mg His6-TEV protease. The dialyzed sample was applied to a GE HisTrap HP 5 mL. The flow-through containing Chd1 was concentrated using an Amicon Millipore 15 ml 50,000 MWCO centrifugal concentrator and applied to a GE S200 16/600 pg size exclusion column, pre-equilibrated in gel filtration buffer (300 mM NaCl, 20 mM Na•HEPES pH 7.4, 10% glycerol (v/v), 1 mM DTT). Peak fractions were concentrated to ~100 μM, aliquoted, flash frozen, and stored at -80 °C. Typical yields of *S. cerevisiae* Chd1 from 1.2 L of insect cell culture are 7-10 mg.

FACT was purified as above, with minor modifications. After dialysis, the sample was applied to tandem GE HisTrap HP 5 mL, GE HiTrap Q 5 mL columns. After washing with 5 CV of dialysis buffer, the HisTrap was removed. FACT was eluted from the HiTrap Q 5 mL by applying a gradient of 0-100% high salt buffer (1 M NaCl, 20 mM Na•HEPES pH 7.4, 10% glycerol (v/v), 1 mM DTT, 30 mM imidazole pH 8.0). Peak fractions were pooled and applied to a GE S200 16/600 pg size exclusion column. Pure fractions containing full-length FACT were concentrated as described above to a concentration of 60 μM, aliquoted, flash

frozen, and stored at -80 °C. Typical preparations yield 10-15 mg of full-length *S. cerevisiae* FACT (Spt16 + Pob3) from 1.2 L of insect cell culture. *S. cerevisiae* Paf1C (ΔCtr9-913) was expressed and purified as described35.

Xenopus laevis histones were expressed and purified as described previously36,37. Briefly, inclusion bodies were resuspended by using a manual Dounce tissue grinder (Sigma-Aldrich). Histones were aliquoted, flash-frozen, lyophilized, and stored at -80 °C prior to use. Lyophilized histones were resuspended in unfolding buffer (7 M guanidine hydrochloride, 20 mM Tris-HCl pH 7.5, 10 mM DTT) to a concentration of 1.5 mg/mL. H2A, H2B, H3, and H4 were then combined at a molar ratio of 1.2:1.2:1:1. The sample was incubated on ice for 30 minutes before it was dialyzed against 3 x 600 mL refolding buffer (2 M NaCl, 10 mM Tris-HCl pH 7.5, 1 mM EDTA pH 8, 5 mM β-mercaptoethanol) for a total of 18 hours at 4 °C. Dialyzed sample was recovered and applied to a GE S200 16/600 pg size exclusion column, pre-equilibrated in refolding buffer. Peak fractions containing histone octamer were pooled and concentrated to 30 μM.

Preparation of nucleosomal complexes

DNA fragments for nucleosome reconstitution were generated by PCR (Extended Data Fig. 3g), essentially as described previously38. A vector containing the Widom 601 sequence was used as a template for PCR. In-house expressed and purified Phusion polymerase was used for the PCR reaction with two primers (Forward: CGCTGTTTTCGAATTTACCCTT TATGCGCCGGTATTGAACCACGCTTATGCCCAGCATCGTTAATCGATGTATATATCT GACACGTGCCT, Reverse: ATCAGAATCCCGGTGCCGAG). The PCR program had the following steps: 1. 98 ° for 1 min, 2. 98 °C for 10 sec, 3. 72 °C for 45 sec, cycle between step 2 and 3 for 35 times, 4. 72 °C for 10 min, 5. Pause at 5 °C. PCR products were pooled from three 48-well PCR plates (100 μL per well). The products were ethanol precipitated and resuspended in 1 mL TE buffer (10 mM Tris pH 8.0, 1 mM EDTA pH 8.0). The resuspended DNA was applied to a ResourceQ 6 mL (GE Healthcare) and eluted with a gradient from 0-100 % TE high salt buffer (10 mM Tris pH 8.0, 1 M NaCl, 1 mM EDTA pH 8.0). Peak fractions were analyzed on a 1 % (v/v) TAE agarose gel and fractions containing the desired DNA product were pooled. The sample was ethanol precipitated, resuspended in 200 μL TE buffer, and stored at -20 ° prior to use.

Nucleosome reconstitution was performed as described37, with minor modifications. Histone octamer and DNA were mixed at a 1:1 molar ratio in 2 M KCl, and transferred to Slide-A-Lyzer MINI Dialysis Units 20,000 MWCO (Thermo Scientific, Waltham, MA, United States). The sample was gradient dialyzed against low salt buffer (30 mM KCl, 20 mM Na•HEPES pH 7.5, 1 mM EDTA pH 8, 1 mM DTT) over 18 hours. The sample was dialyzed for another four hours against low salt buffer, recovered, and stored at 4 °C. Quantification of the reconstituted nucleosome was achieved by measuring absorbance at 280 nm. Molar extinction coefficients were determined for protein and nucleic acid components and were summed to yield a molar extinction coefficient for the reconstituted NCP.

To prepare a nucleosome-Chd1-FACT-Paf1C complex, FACT, Chd1, and Paf1C were mixed at a molar ratio of 1:1.2:1.4 and incubated for 10 minutes. Zero monovalent salt buffer (2

mM $MgCl_2$, 20 mM Na•HEPES pH 7.5, 5 % glycerol (v/v), 1 mM DTT). was added within 6 minutes to achieve a final monovalent salt concentration of 30 mM. Reconsituted NCP was added at a 0.5 molar ratio of the FACT concentration. The sample was incubated for 10 minutes, centrifuged (21,000xg, 4 °C, 10 min), and applied to a Superose 6 Increase 3.2/300 column equilibrated in gel filtration buffer (30 mM NaCl, 2 mM $MgCl_2$, 20 mM Na•HEPES pH 7.5, 5 % glycerol (v/v), 1 mM DTT). Peak fractions were pooled, ADP·BeF_3 was added to a concentration of 1 mM ADP and 3 mM BeF_3^-, and incubated for 10 minutes. The sample was cross-linked with 0.1 % (v/v) glutaraldehyde, incubated for 10 minutes on ice. The cross-linking reaction was quenched for 10 min using a concentration of 90 mM Tris-HCl (pH 7.9), 9 mM lysine and 9 mM aspartate. The sample was transferred to a Slide-A-Lyzer MINI Dialysis Unit 20,000 MWCO (Thermo Scientific), and dialyzed for 6 hours against 600 mL dialysis buffer (30 mM NaCl, 2 mM $MgCl_2$, 20 mM Na•HEPES pH 7.4, 1 mM DTT).

Cryo-EM and image processing

The nucleosome-Chd1-FACT-Paf1C complex sample was applied to R2/2 gold grids (Quantifoil). The grids were glow-discharged for 45 seconds before sample application of 2 μL on each side of the grid. The sample was subsequently blotted for 8.5 seconds and vitrified by plunging into liquid ethane with a Vitrobot Mark IV (FEI Company, Hillsboro, OR, United States) operated at 4 °C and 100 % humidity. Cryo-EM data was acquired on a FEI Titan Krios transmission electron microscope (TEM) operated at 300 keV, equipped with a K2 summit direct detector (Gatan, Pleasanton, CA, United States). Automated data acquisition was carried out using FEI EPU software at a nominal magnification of 105,000x. Image stacks of 40 frames were collected in counting mode over 10s. The dose rate was 3 e^- per Ångström^2 per second for a total dose of 30 e^- $Å^{-2}$. A total of 3806 image stacks were collected.

Frames were stacked and subsequently processed with MotionCor239. CTF correction was performed with Gctf40. Image processing was performed with RELION 2.0.441,42, unless noted otherwise. Post-processing of refined models was performed with automatic B-factor determination in RELION. Particles were picked using projections of an initial reconstruction (~400,000 particles, FEI Falcon 2, not shown), yielding 990,020 particle images. Particles were extracted with a box size of 224^2 pixel, normalized, and screened using iterative rounds of reference-free 2D classification, yielding a total of 773,326 particles (Extended data Fig. 1). Particle images were sub-divided into three batches and processed individually. Using a 40 Å low-pass filtered model from an initial reconstruction (not shown), we performed iterative rounds of hierarchical 3D classification with image alignment as outlined in Extended Data Fig. 1c. The three particle image batches were subsequently merged, re-extracted with a box size of 240^2 pixel and subjected to another round of 3D classification with image alignment. The best two classes were combined and subjected to a 3D refinement with a mask that encompasses the entire NCP-Chd1 complex. The NCP-Chd1 reconstruction was obtained from 67,032 particles with a resolution of 4.8 Å (gold-standard Fourier shell correlation 0.143 criterion). The map was sharpened with a B-factor of -204 $Å^2$. Local resolution estimates were determined using a sliding window of 40^3 voxels as previously described43. Resolutions for individual Chd1 domains were determined

by masking the respective regions and perfoming B-factor sharpening (gold-standard Fourier shell correlation 0.143 criterion) using RELION.

Model building

Crystal structures of the *X. laevis* nucleosome with Widom 601 sequence11 (PDB code 3LZ0), the *S. cerevisiae* Chd1 DNA-binding domains13 (PDB code 3TED), and *S. cerevisiae* Chd1 core12 (double chromodomain and ATPase motor, PDB code 3MWY) were placed into the electron density using UCSF Chimera44. The individual Chd1 domains (SANT, SLIDE, double chromodomain, ATPase lobe1, ATPase lobe2) were fitted as rigid bodies. Residues 842-922 were removed from the double chromodomain-ATPase motor structure (PDB code 3MWY) due to weak density. We did not observe assignable density for the CHCT domain of Chd1. We did not assign weak density near H3 (residues 46-56), and H2A (residues 56-71). Extranucleosomal DNA, nucleosomal DNA from SHL -7 to SHL-5, and the H4 N-terminal tail residues 16-20 were built using COOT45. Three rounds of flexible fitting were performed with vmd46 and MDFF47, resulting in good fits of the electron density. Secondary structure restraints were applied and the model was real-space refined against the post-processed EM map using PHENIX48. ADP·BeF_3 was built by superpositioning ATP-gamma-S from the inactive Chd1 structure (PDB code 3MWY) onto our model, and replacing the ATP analogue with ADP·BeF_3 (PDB code 3ICE)49. BeF_3^- was modeled in a tetrahedral conformation for simplicity but is likely planar when it mimics part of the pentavalent transition state of ATP hydrolysis. While ADP is remarkably well-resolved at the given resolution, BeF_3^- has weaker density and was modelled based on previous structural data from other ATPases. R804 and R807 were fitted manually. The complete structure was geometry-optimized with PHENIX. Figures were generated using PyMol50 and UCSF Chimera44. Electron density was shown for the local resolution filtered map, if not stated otherwise.

Data availability statement

The electron density reconstruction and final model were deposited with the EM Data Base (accession code EMDB-3765) and with the Protein Data Bank (accession code 5O9G).

Europe PMC Funders Author Manuscripts

Europe PMC Funders Author Manuscripts

Extended Data

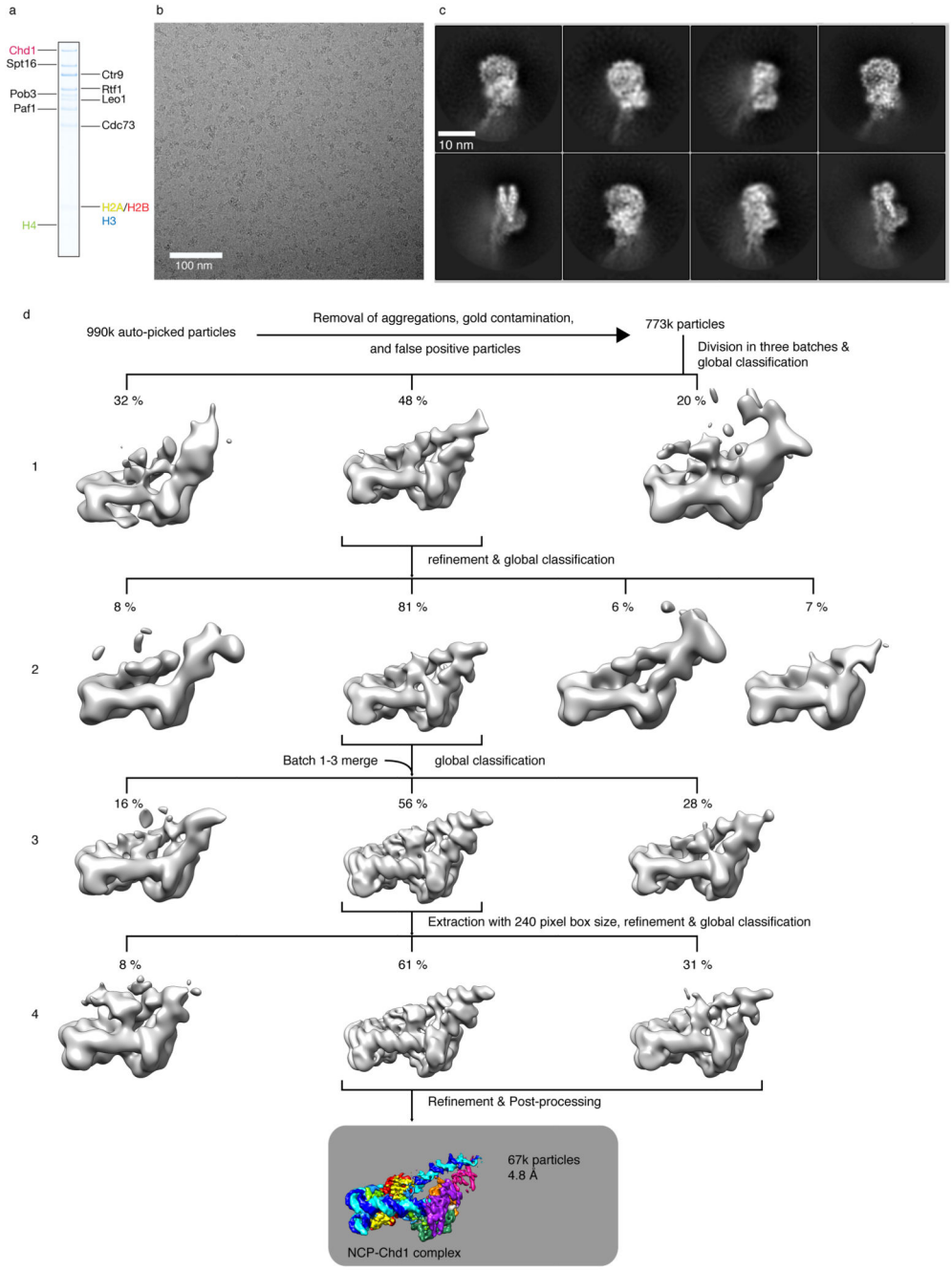

Extended Data Figure 1. Cryo-EM structure determination and analysis.

a. Formation of the nucleosome-Chd1-FACT-Paf1C complex. SDS-PAGE of peak fraction used for cryo-EM grid preparation containing Chd1, FACT subunits, Paf1C subunits and histones. Identity of the bands was confirmed by mass spectrometry. For gel source data, see Supplementary Figure 1.

b. Representative cryo-EM micrograph of data collection.

c. 2D class averages contain nucleosome-like shapes.

d. Sorting and classification tree used to reconstruct the nucleosome-Chd1 particle at 4.8 Å resolution. Steps 1 and 2 of batch 1 global classification are shown representatively for all three batches.

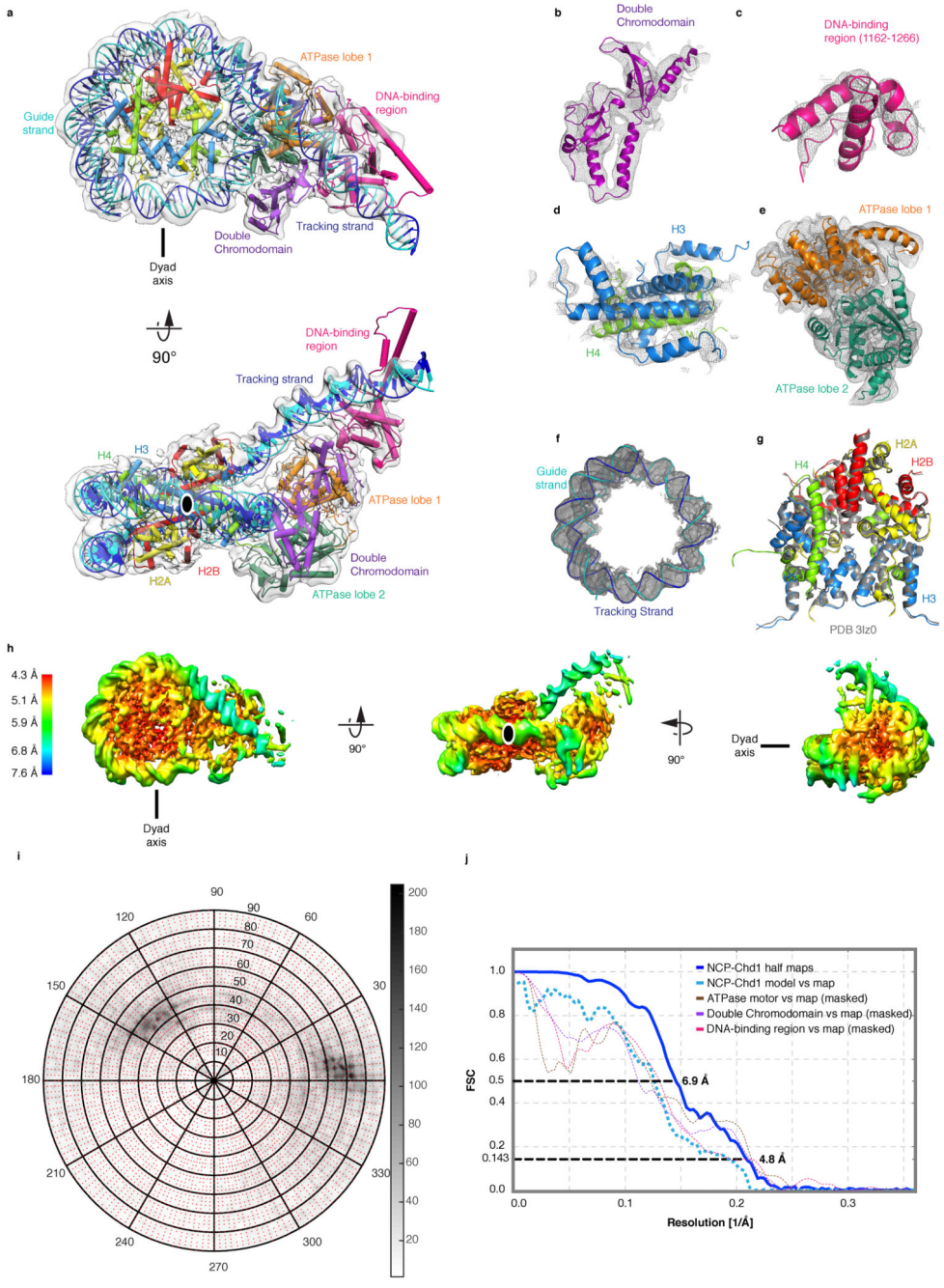

Extended Data Figure 2. Quality of the nucleosome-Chd1 structure.

a. Overall fit of the nucleosome-Chd1 structure to the electron density. Two views are depicted as in Fig. 1b, c.

Europe PMC Funders Author Manuscripts

b-f. Electron density (grey mesh) for various Chd1 domains reveals secondary structure and a good fit for DNA (SHL -4 to SHL +7).

g. Superposition of the histone octamer core with canonical octamer core (PDB code 3LZ0). The canonical octamer core is rendered in grey.

h. Nucleosome-Chd1 reconstruction colored according to local resolution43.

i. Angular distribution of particles. Red dots indicate the presence of at least one particle image assigned within ±1°. Shading from white to black indicates the density of particle images at a given orientation.

j. Estimation of the average resolution. The dark blue line indicates the Fourier shell correlation between the half maps of the reconstruction. The dotted light blue line indicates the Fourier shell correlation between the derived model and the reconstruction. Resolutions are given for the FSC 0.143 and the FSC 0.5 criterion. The dotted lines show the Fourier shell correlation between the derived Chd1 domains and the corresponding masked regions.

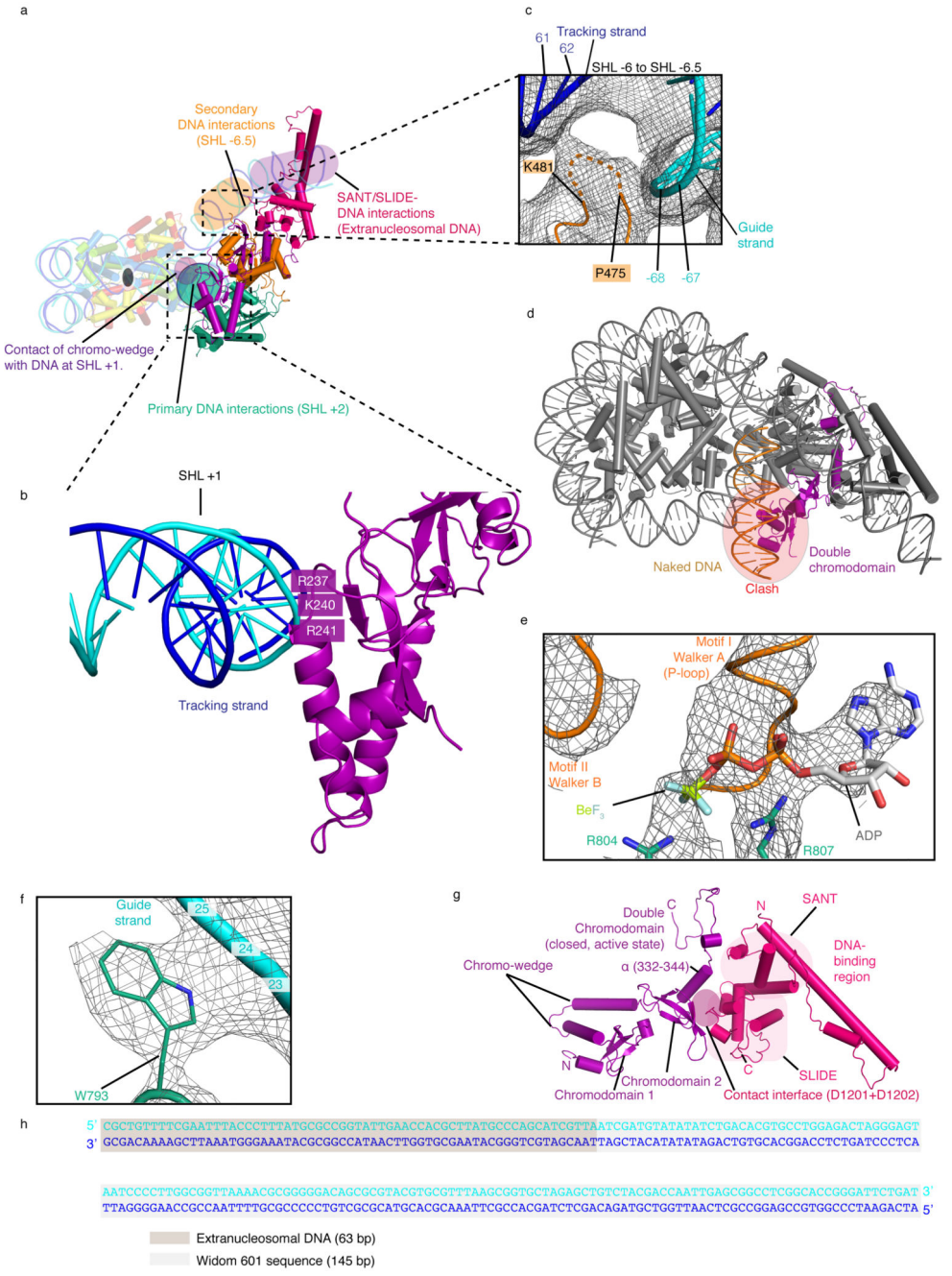

Extended Data Figure 3. Chd1-DNA interactions and Chd1 interaction interfaces.

a. Overview of Chd1-DNA interactions.

b. Contact of chromo-wedge with DNA at SHL +1.

c. Secondary DNA contacts of ATPase. Contact of motif Ib with first DNA gyre around SHL -6.

d. Modeling linear B-DNA (orange) onto the ATPase motor in the nucleosome-Chd1 structure leads to a clash with the double chromodomain (purple). B-DNA was superimposed onto nucleosomal DNA at SHL +2.

Europe PMC Funders Author Manuscripts

e. ADP·BeF_3 binds in the active site of the Chd1 ATPase motor. Electron density is shown for ADP·BeF_3, motif I (Walker A, P-loop, residues 403-410), motif II (Walker B, residues 510-515), and the arginine fingers (R804 + R807). Motifs I and II are shown in ribbon representation. ADP·BeF_3 and the arginine finger residues are shown as sticks. Density for ADP is strong, whereas density for BeF_3^- is weaker and thus we cannot formally rule out that BeF_3^- is not bound or shows only partial occupancy.

f. Contact of W793 with the phosphate backbone of the guide strand at SHL +2. Electron density is shown as a grey mesh. Side chain of W793 is shown as a stick representation.

g. Interface between the double chromodomain and the SANT/SLIDE domains of the DNA binding region. Chd1 domains are colored as in Fig. 1a.

h. Sequence of the Widom 601 sequence with 63 bp of extranucleosomal DNA.

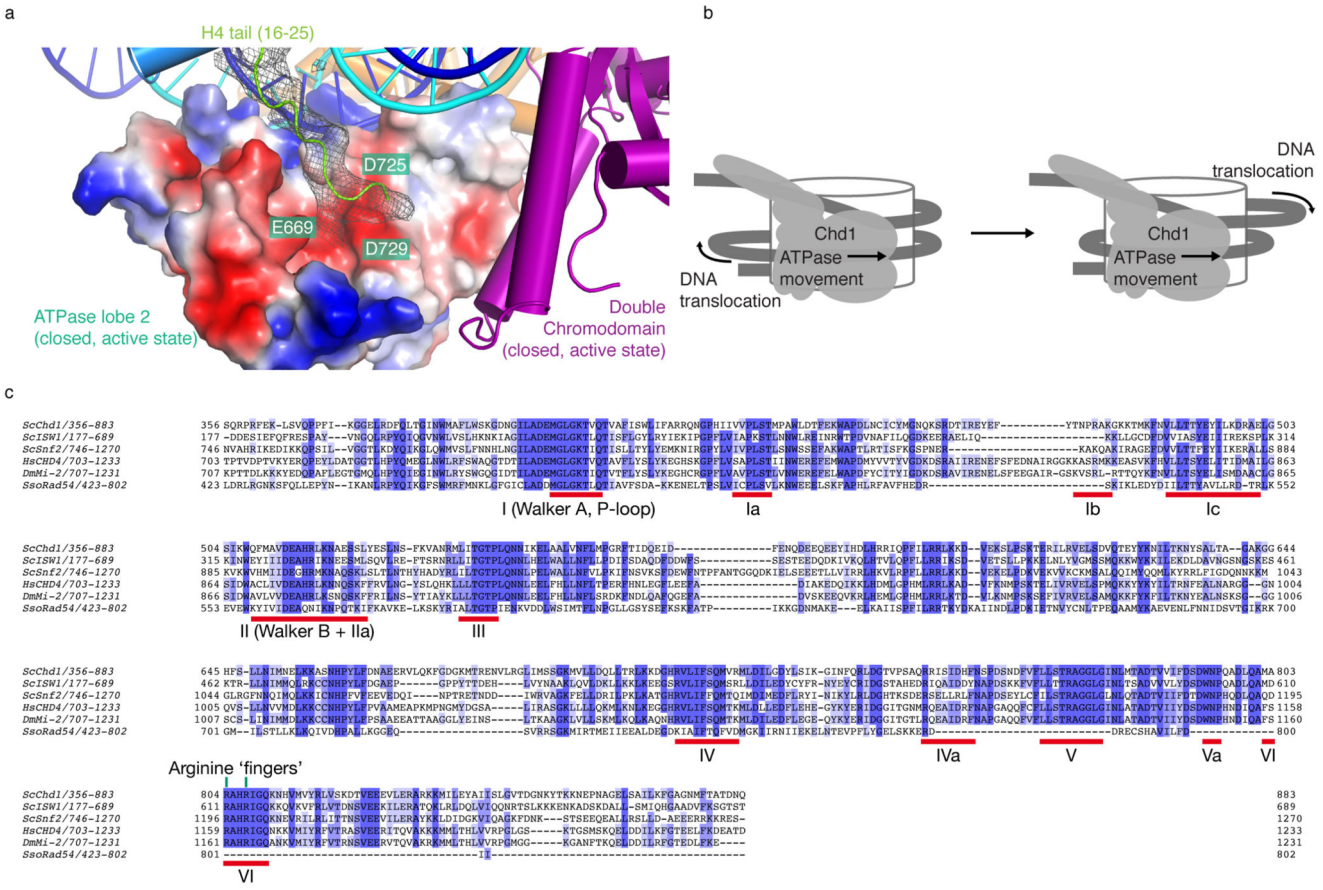

Extended Data Figure 4. ATPase conservation and histone H4 tail binding.

a. Chd1 binds the N-terminal tail of histone H4 (green) with ATPase lobe 2 (surface representation coloured according to electrostatic surface potential; red, negative, white, neutral, blue, positive). The view is the inverse of that in Fig. 1b, i.e. after a 180° rotation.

b. Chd1 ATPase activity results in DNA translocation towards the octamer dyad, loosening DNA gyre 1 and triggering nucleosome remodelling.

c. Sequence alignment of ATPase regions in *Sc*Chd1 (356-883), *Sc*Isw1 (177-689), *Sc*Snf2 (746-1270), *Hs*Chd4 (703-1233), *Dm*Mi-2 (707-1231), and *Sso*Rad54 (423-802). Arginine

'fingers' of *Sc*Chd1 (R804+R807) are indicated and ATPase motifs are underlined. Sequence coloured according to identity. Darker shades of blue indicate higher conservation, whereas lighter shades of blue indicate less conservation. Alignment was generated with MAFFT51 and visualized using JalView52.

Extended Data Table 1

Cryo-EM data collection, refinement and validation statistics

	Nucleosome-Chd1 structure (EMDB-3765) (PDB 5Q9G)
Data collection and processing	
Microscope	FEI Titan Krios
Detector	Gatan K2 Summit
Magnification	105,000X
Voltage (kV)	300
Electron exposure (e–/Å^2)	30
Defocus range (μm)	1.25 to 2.75
Pixel size (Å)	1.35
Symmetry imposed	C1
Initial particle images (no.)	990,020
Final particle images (no.)	67,032
Map resolution (Å)	4.8
FSC threshold	0.143
Refinement	
Initial models used (PDB code)	3LZ0, 3MWY, 3TED
Map sharpening *B* factor (Å^2)	-204
Model composition	
Non-hydrogen atoms	19667
Protein residues	1934
Ligands	2
Validation	
MolProbity score	1.93
Clashscore	7
Poor rotamers (%)	0.36
Ramachandran plot	
Favored (%)	90.81
Allowed (%)	9.06
Disallowed (%)	0.13

Supplementary Material

Refer to Web version on PubMed Central for supplementary material.

Europe PMC Funders Author Manuscripts

Acknowledgements

We thank past and present members of the Cramer laboratory including Franz Fischer, Rebecca Kohler, Simon Neyer, Dimitry Tegunov, and Youwei Xu. We thank the Halic lab for *X. laevis* histone expression plasmids, a plasmid containing the Widom 601 sequence, and initial advice on histone purification. SMV was supported by an EMBO Long-Term-Fellowship (ALTF 745-2014). PC was supported by the Deutsche Forschungsgemeinschaft (SFB860, SPP1935), the European Research Council Advanced Investigator Grant TRANSREGULON (grant agreement No 693023), and the Volkswagen Foundation.

References

1. Narlikar GJ, Sundaramoorthy R, Owen-Hughes T. Mechanisms and Functions of ATP-Dependent Chromatin-Remodeling Enzymes. Cell. 2013; 154:490–503. [PubMed: 23911317]
2. Delmas V, Stokes DG, Perry RP. A mammalian DNA-binding protein that contains a chromodomain and an SNF2/SWI2-like helicase domain. PNAS. 1993; 90:2414–2418. [PubMed: 8460153]
3. Lieleg C, et al. Nucleosome spacing generated by ISWI and CHD1 remodelers is constant regardless of nucleosome density. Mol Cell Biol. 2015; 35:1588–1605. [PubMed: 25733687]
4. Hughes AL, Rando OJ. Comparative Genomics Reveals Chd1 as a Determinant of Nucleosome Spacing in Vivo. G3 (Bethesda). 2015; 5:1889–1897. [PubMed: 26175451]
5. Lusser A, Urwin DL, Kadonaga JT. Distinct activities of CHD1 and ACF in ATP-dependent chromatin assembly. Nat Struct Mol Biol. 2005; 12:160–166. [PubMed: 15643425]
6. Skene PJ, Hernandez AE, Groudine M, Henikoff S. The nucleosomal barrier to promoter escape by RNA polymerase II is overcome by the chromatin remodeler Chd1. eLife. 2014; 3:e02042. [PubMed: 24737864]
7. Gaspar-Maia A, et al. Chd1 regulates open chromatin and pluripotency of embryonic stem cells. Nature. 2009; 460:863–868. [PubMed: 19587682]
8. Liu X, Li M, Xia X, Li X, Chen Z. Mechanism of chromatin remodelling revealed by the Snf2-nucleosome structure. Nature. 2017; 544:440–445. [PubMed: 28424519]
9. Nodelman IM, et al. Interdomain Communication of the Chd1 Chromatin Remodeler across the DNA Gyres of the Nucleosome. Mol Cell. 2017; 65:447–459.e6. [PubMed: 28111016]
10. Lowary PT, Widom J. New DNA sequence rules for high affinity binding to histone octamer and sequence-directed nucleosome positioning. J Mol Biol. 1998; 276:19–42. [PubMed: 9514715]
11. Vasudevan D, Chua EYD, Davey CA. Crystal structures of nucleosome core particles containing the '601' strong positioning sequence. J Mol Biol. 2010; 403:1–10. [PubMed: 20800598]
12. Hauk G, McKnight JN, Nodelman IM, Bowman GD. The Chromodomains of the Chd1 Chromatin Remodeler Regulate DNA Access to the ATPase Motor. Mol Cell. 2010; 39:711–723. [PubMed: 20832723]
13. Sharma A, Jenkins KR, Heroux A, Bowman GD. Crystal structure of the chromodomain helicase DNA-binding protein 1 (Chd1) DNA-binding domain in complex with DNA. J Biol Chem. 2011; 286:42099–42104. [PubMed: 22033927]
14. Mohanty B, Helder S, Silva APG, Mackay JP, Ryan DP. The Chromatin Remodelling Protein CHD1 Contains a Previously Unrecognised C-Terminal Helical Domain. J Mol Biol. 2016; :1–17. DOI: 10.1016/j.jmb.2016.08.028
15. Sundaramoorthy R, et al. Structural reorganization of the chromatin remodeling enzyme Chd1 upon engagement with nucleosomes. eLife. 2017; 6:e22510–28. [PubMed: 28332978]
16. Sinha KK, Gross JD, Narlikar GJ. Distortion of histone octamer core promotes nucleosome mobilization by a chromatin remodeler. Science. 2017; 355:eaaa3761. [PubMed: 28104838]
17. McKnight JN, Jenkins KR, Nodelman IM, Escobar T, Bowman GD. Extranucleosomal DNA binding directs nucleosome sliding by Chd1. Mol Cell Biol. 2011; 31:4746–4759. [PubMed: 21969605]
18. Bednar J, et al. Structure and Dynamics of a 197 bp Nucleosome in Complex with Linker Histone H1. Mol Cell. 2017; 66:384–397.e8. [PubMed: 28475873]

Europe PMC Funders Author Manuscripts

19. Gu M, Rice CM. Three conformational snapshots of the hepatitis C virus NS3 helicase reveal a ratchet translocation mechanism. Proc Natl Acad Sci USA. 2010; 107:521–528. [PubMed: 20080715]
20. Sengoku T, Nureki O, Nakamura A, Kobayashi S, Yokoyama S. Structural basis for RNA unwinding by the DEAD-box protein Drosophila Vasa. Cell. 2006; 125:287–300. [PubMed: 16630817]
21. Huang S, et al. Recurrent deletion of CHD1 in prostate cancer with relevance to cell invasiveness. Oncogene. 2012; 31:4164–4170. [PubMed: 22179824]
22. Singleton MR, Dillingham MS, Wigley DB. Structure and mechanism of helicases and nucleic acid translocases. Annu Rev Biochem. 2007; 76:23–50. [PubMed: 17506634]
23. Dürr H, Körner C, Müller M, Hickmann V, Hopfner K-P. X-ray structures of the Sulfolobus solfataricus SWI2/SNF2 ATPase core and its complex with DNA. Cell. 2005; 121:363–373. [PubMed: 15882619]
24. Saha A, Wittmeyer J, Cairns BR. Chromatin remodeling through directional DNA translocation from an internal nucleosomal site. Nat Struct Mol Biol. 2005; 12:747–755. [PubMed: 16086025]
25. Saikrishnan K, Powell B, Cook NJ, Webb MR, Wigley DB. Mechanistic basis of 5'-3' translocation in SF1B helicases. Cell. 2009; 137:849–859. [PubMed: 19490894]
26. Hopfner K-P, Michaelis J. Mechanisms of nucleic acid translocases: lessons from structural biology and single-molecule biophysics. Curr Opin Struct Biol. 2007; 17:87–95. [PubMed: 17157498]
27. Wigley DB, Bowman GD. A glimpse into chromatin remodeling. Nature Structural & Molecular Biology. 2017; 24:498–500.
28. Le Gallo M, et al. Exome sequencing of serous endometrial tumors identifies recurrent somatic mutations in chromatin-remodeling and ubiquitin ligase complex genes. Nat Genet. 2012; 44:1310–1315. [PubMed: 23104009]
29. Clapier CR, Längst G, Corona DF, Becker PB, Nightingale KP. Critical role for the histone H4 N terminus in nucleosome remodeling by ISWI. Mol Cell Biol. 2001; 21:875–883. [PubMed: 11154274]
30. Nodelman IM, et al. The Chd1 chromatin remodeler can sense both entry and exit sides of the nucleosome. Nucleic Acids Research. 2016; :gkw406.doi: 10.1093/nar/gkw406
31. Clapier CR, Cairns BR. The biology of chromatin remodeling complexes. Annu Rev Biochem. 2009; 78:273–304. [PubMed: 19355820]
32. Leonard JD, Narlikar GJ. A nucleotide-driven switch regulates flanking DNA length sensing by a dimeric chromatin remodeler. Mol Cell. 2015; 57:850–859. [PubMed: 25684208]
33. Yan L, Wang L, Tian Y, Xia X, Chen Z. Structure and regulation of the chromatin remodeller ISWI. Nature. 2016; 540:466–469. [PubMed: 27919072]
34. Vos SM, et al. Architecture and RNA binding of the human negative elongation factor. eLife. 2016; 5:e14981. [PubMed: 27282391]
35. Xu Y, et al. Architecture of the RNA polymerase II-Paf1C-TFIIS transcription elongation complex. Nat Commun. 2017; 8:15741.
36. Luger K, Rechsteiner TJ, Richmond TJ. Expression and purification of recombinant histones and nucleosome reconstitution. Methods Mol Biol. 1999; 119:1–16. [PubMed: 10804500]
37. Dyer PN, et al. Reconstitution of nucleosome core particles from recombinant histones and DNA. Meth Enzymol. 2004; 375:23–44. [PubMed: 14870657]
38. Maskell DP, et al. Structural basis for retroviral integration into nucleosomes. Nature. 2015; doi: 10.1038/nature14495
39. Zheng SQ, et al. MotionCor2: anisotropic correction of beam-induced motion for improved cryo-electron microscopy. Nat Methods. 2017; 14:331–332. [PubMed: 28250466]
40. Zhang K. Gctf: Real-time CTF determination and correction. J Struct Biol. 2016; 193:1–12. [PubMed: 26592709]
41. Scheres SHW. A Bayesian view on cryo-EM structure determination. J Mol Biol. 2012; 415:406–418. [PubMed: 22100448]

42. Kimanius D, Forsberg BO, Scheres SH, Lindahl E. Accelerated cryo-EM structure determination with parallelisation using GPUs in RELION-2. eLife. 2016; 5:e18722. [PubMed: 27845625]
43. Plaschka C, et al. Transcription initiation complex structures elucidate DNA opening. Nature. 2016; doi: 10.1038/nature17990
44. Pettersen EF, et al. UCSF Chimera--a visualization system for exploratory research and analysis. J Comput Chem. 2004; 25:1605–1612. [PubMed: 15264254]
45. Emsley P, Lohkamp B, Scott WG, Cowtan K. Features and development of Coot. Acta Crystallogr D Biol Crystallogr. 2010; 66:486–501. [PubMed: 20383002]
46. Humphrey W, Dalke A, Schulten K. VMD: visual molecular dynamics. J Mol Graph. 1996; 14 33–8–27–8.
47. Trabuco LG, Villa E, Mitra K, Frank J, Schulten K. Flexible fitting of atomic structures into electron microscopy maps using molecular dynamics. Structure. 2008; 16:673–683. [PubMed: 18462672]
48. Adams PD, et al. PHENIX: a comprehensive Python-based system for macromolecular structure solution. Acta Crystallogr D Biol Crystallogr. 2010; 66:213–221. [PubMed: 20124702]
49. Thomsen ND, Berger JM. Running in reverse: the structural basis for translocation polarity in hexameric helicases. Cell. 2009; 139:523–534. [PubMed: 19879839]
50. Schrodinger LLC. The PyMOL Molecular Graphics System, Version 1.8. 2015.
51. Katoh K, Standley DM. MAFFT multiple sequence alignment software version 7: improvements in performance and usability. Mol Biol Evol. 2013; 30:772–780. [PubMed: 23329690]
52. Waterhouse AM, Procter JB, Martin DMA, Clamp M, Barton GJ. Jalview Version 2--a multiple sequence alignment editor and analysis workbench. Bioinformatics. 2009; 25:1189–1191. [PubMed: 19151095]

Europe PMC Funders Author Manuscripts

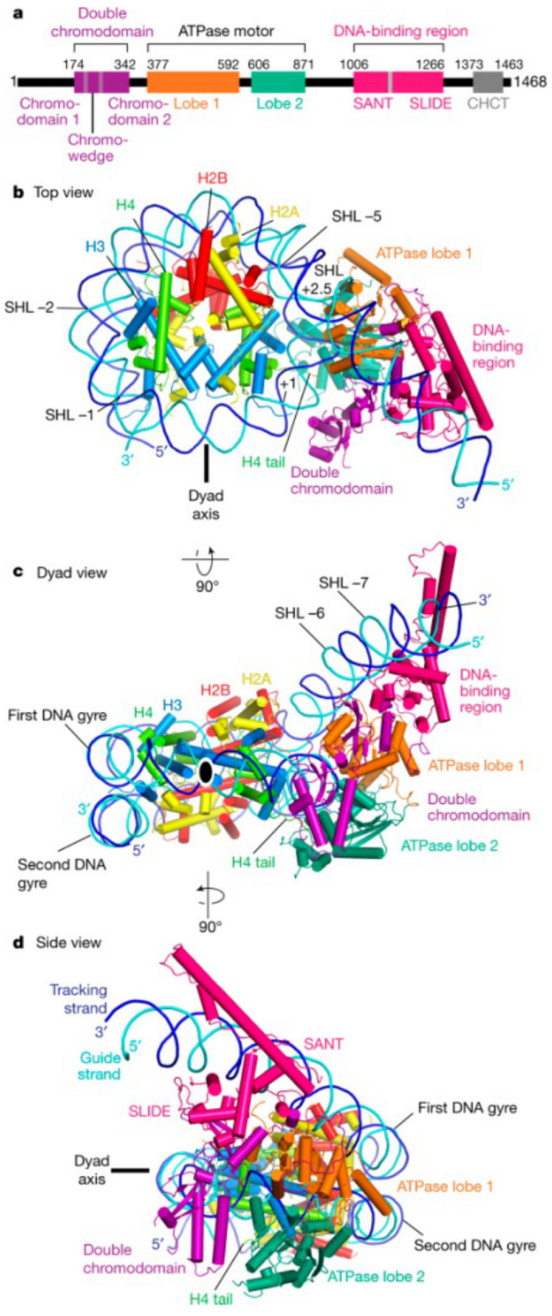

Figure 1. Structure of nucleosome-Chd1 complex.

a. Chd1 domain architecture. Residues at domain boundaries are indicated.

b-d. Three views of the structure. Chd1 domains are colored as in (a). H2A, H2B, H3, H4, tracking strand, and guide strand are in yellow, red, light blue, green, dark blue, and cyan, respectively. The histone octamer dyad axis is indicated as black line or black oval circle. SHL, superhelical location.

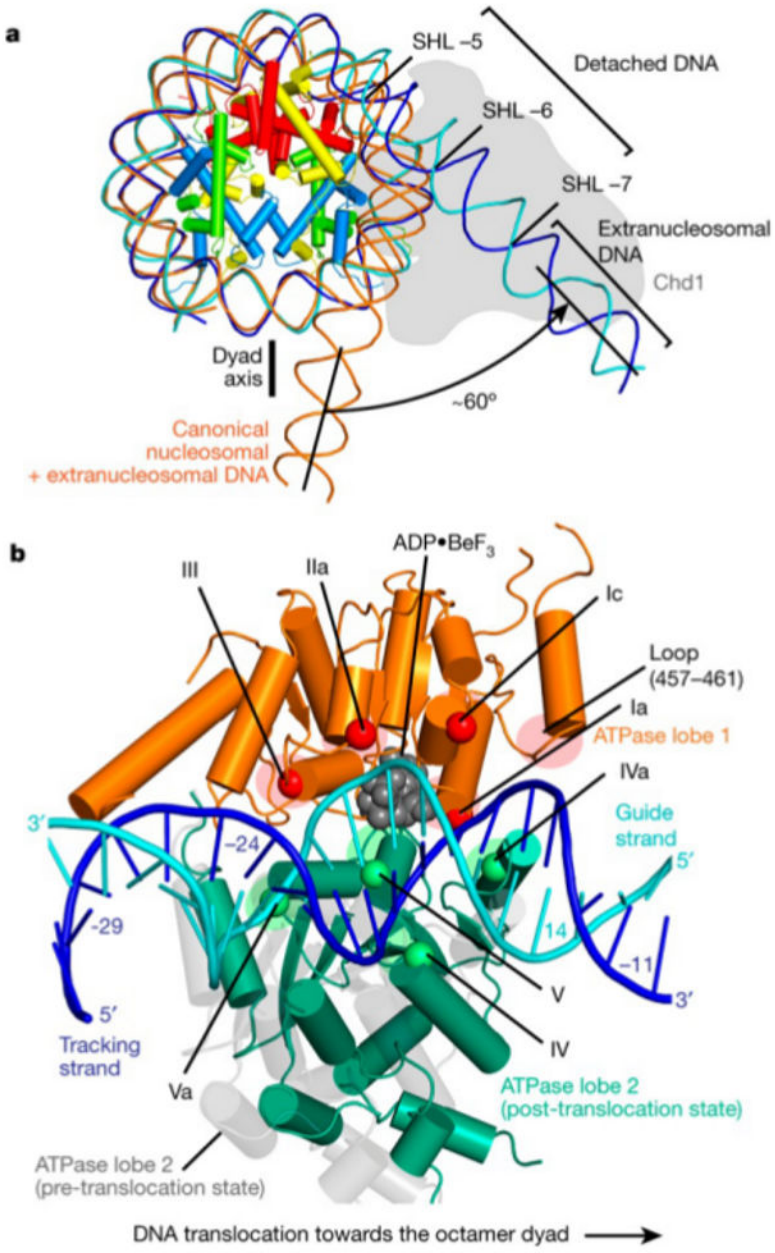

Figure 2. Chd1-DNA interactions.

a. Detachment of nucleosomal DNA from the histone octamer at SHL -7 to -5. Extranucleosomal DNA rotates by ~60º with respect to its location in the absence of Chd1 (orange, modelled by extending nucleosomal DNA with B-DNA). The position of Chd1 is indicated in grey color.

b. Primary ATPase-DNA interactions. Location of ATPase motifs on lobe 1 and lobe 2 are highlighted in red and green, respectively. The view is from the center of the histone octamer onto nucleosomal DNA. DNA register is indicated by numbering next to DNA bases. Color code is as in Fig. 1. ADP·BeF_3 is shown as grey spheres. The model of lobe 2 in the pre-

translocated position (grey) was derived from superposition of the nucleosome-Snf2 structure (PDB code 5X0Y)8.

Europe PMC Funders Author Manuscripts

Europe PMC Funders Author Manuscripts

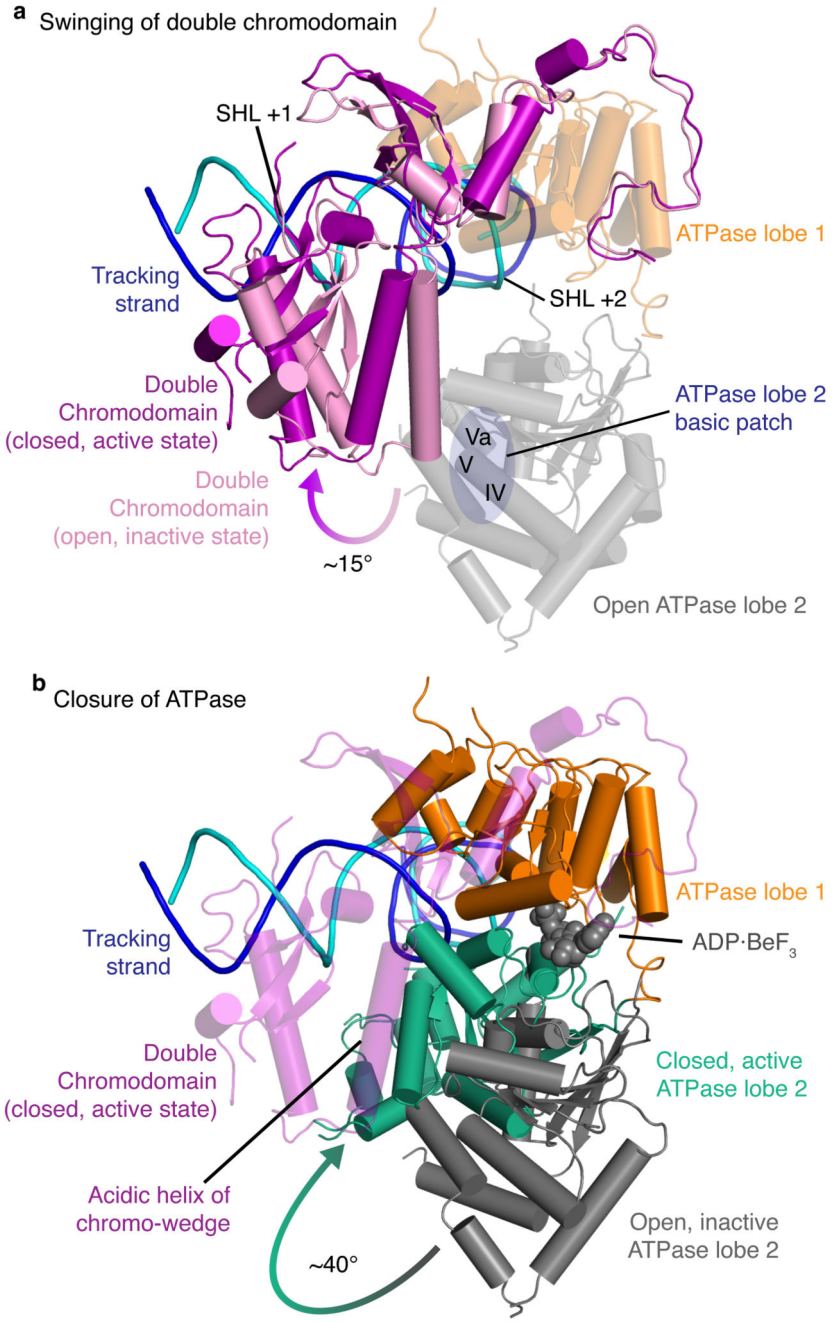

Figure 3. Chd1 structural changes and ATPase activation.

a. Swinging of double chromodomain (open state, light pink; closed state, purple) onto DNA liberates ATPase lobe 2 (grey). The structure of free Chd1 in its inactive state12 (PDB code 3MWY) was placed by superimposing ATPase lobe 1 (orange). In the inactive state, the chromo-wedge binds to a basic patch on lobe 2. View as in Fig. 1c.

b. ATPase closure and activation. Lobe 2 (sea green) rotates by ~40º to allow for binding of ADP·BeF_3 (grey spheres). BeF_3^- was modeled in a tetrahedral conformation for simplicity but is likely planar when it mimics part of the pentavalent transition state of ATP hydrolysis.

Europe PMC Funders Author Manuscripts